JBIS, Vol. 53, pp. 26-38, 2000

AUTONOMOUS PATH PLANNING FOR ON-ORBIT SERVICING VEHICLES

COLIN R. McINNES
Department of Aerospace Engineering, University of Glasgow, G12 8QQ, Scotland, UK.

On-orbit servicing has long been considered as a means of reducing mission costs. While automated on-orbit servicing of satellites in LEO and GEO has yet to be realised, the International Space Station (ISS) will require servicing in a number of forms for re-supply, external visual inspection and maintenance. This paper will discuss a unified approach to path planning for such servicing vehicles using artificial potential field methods. In particular, path constrained rendezvous and docking of the ESA Automated Transfer Vehicle (ATV) at the ISS will be investigated as will mission and path planning tools for the Daimler-Chrysler Aerospace ISS Inspector free-flying camera. Future applications for free-flying microcameras and co-operative control between multiple free-flyers for on-orbit assembly will also be considered.

1. INTRODUCTION

Future mission applications for on-orbit servicing vehicles include re-supply, inspection and maintenance of the International Space Station (ISS) and inspection and maintenance of Geostationary satellites, along with more advance tasks such as on-orbit assembly. A key technology for these missions is the provision of automated path planning tools. Manual control of free-flying vehicles is a demanding task requiring simultaneous control of 3 translational and 3 rotational degrees of freedom. Such manual control becomes even more challenging for proximity operations near large and complex space structures such as the ISS. Automated path planning can be used as a pre-flight tool to plan a series of events on a time-line, or for real-time control using the spacecraft flight computer. As will be seen, methods have been developed for both of these problems: real-time control to enable active collision avoidance for the ATV and path planning for the ISS Inspector.

Conventional approaches to spacecraft autonomy have centred on artificial intelligence or expert systems (see for example ref. [1]) to enable real-time, on-board guidance and control. Other approaches have utilised fuzzy logic and neural networks. While successful, these approaches have limitations which motivates the investigation of alternative methods. In particular expert systems require significant on-board software to implement, which imposes increased loads on limited flight computers. Similarly, neural network methods can provide autonomous control but are difficult to explicitly validate for safety critical applications.

A new approach to autonomous control is presented which is computationally efficient, can be mathematically validated and has a wide range of applications. The method, which has its origins in terrestrial robotics (see for example ref. [2]), hinges on defining an artificial potential field which represents the environment in which the spacecraft is to manoeuvre. The potential field is configured to have a global minimum at the desired terminal state of the vehicle and has regions of high potential which represent path constraints. The spacecraft controls are then chosen such that the rate of descent of the potential field along the spacecraft trajectory is always rendered negative definite. Therefore, according to Lyapunov's theorem [3], for a suitable potential field this ensures that the vehicle converges to the desired terminal state without violating predefined path constraints. It will be demonstrated that the method may be conveniently formulated for continuous and discrete control and for the co-operative control of multiple spacecraft.

For many applications the controls provided by the method are available in a simple analytic form

Presented at the British Interplanetary Society Symposium "Reducing Space Mission Cost" held on 14 April 1999.

so that the computational burden for real-time implementation is small. Furthermore, due to the ease with which path constraints are included, complex manoeuvres can be undertaken using these rather simple control laws. The control laws can be explicitly validated using Lyapunov's theorem so that the method can be guaranteed for safety critical applications. Therefore, due to the benefits and flexibility of the method, it appears to form the basis for an autonomous control method for a number of applications. This form of the potential field method will be investigated in some detail for ATV proximity operations at the ISS.

While some forms of the potential field method are appropriate for on-board application, geometrically complex problems require numerical methods to generate the potential field and calculate its local gradient [4]. For these more numerically intensive problems the method is more appropriate for pre-flight mission planning. In this case a path planner generates a series of way points which are tracked by a separate real-time controller. This form of the potential field method will be investigated for operations of the Inspector vehicle in the vicinity of the ISS. In addition to path planning tools, visualisation tools have also been developed for Inspector to aid in the choice of appropriate visual inspection locations. Lastly, co-operative control of groups of free-flying vehicles will be explored for future on-orbit assembly problems.

2. POTENTIAL FIELD METHODS

2.1 Continuous Control

Before specific mission applications are considered, various formulations of the potential field method will be discussed [5]. In this section problems with continuous control action will be considered. Such problems relate to, for example, orbit control using continuous low thrust propulsion or quasi-continuous propulsion using pulse-modulated thrusters. A generic non-linear dynamical system will be considered with generalised position vector $\mathbf{x}$ and generalised velocity vector $\mathbf{v}$. The dynamical system will be taken to have the following structure

$$\dot{\mathbf{x}} = \mathbf{v} \tag{1a}$$

$$\dot{\mathbf{v}} = \mathbf{f}(\mathbf{x}, \mathbf{v}, t; \boldsymbol{\alpha}) \tag{1b}$$

where the vector $\boldsymbol{\alpha}$ represents spacecraft actuator inputs to implement the required control commands.

A potential field will now be defined by a scalar function $\phi(\mathbf{x},\mathbf{v};\boldsymbol{\lambda})$ where $\boldsymbol{\lambda}$ is a vector of free parameters which may be used to shape the field. Normally this function may be decomposed into a true potential term V containing position elements only and a simple velocity term used to drive the system to rest at the terminal state, viz.

$$\phi = \tfrac{1}{2}\mathbf{v}.\mathbf{v} + V(\mathbf{x};\boldsymbol{\lambda}) \tag{2}$$

Using the chain rule to obtain the total time derivative, the rate of descent of the potential function can be written as

$$\dot{\phi} = \mathbf{v}.\dot{\mathbf{v}} + \nabla V(\mathbf{x};\boldsymbol{\lambda}).\mathbf{v} \tag{3}$$

Then, an appropriate choice of acceleration will render the rate of descent of the potential function negative definite, viz.

$$\dot{\mathbf{v}} = -\kappa(\mathbf{x},\mathbf{v})\mathbf{v} - \nabla V(\mathbf{x},\boldsymbol{\lambda}) \tag{4}$$

Using this acceleration command the rate of descent of the potential function is then found to be

$$\dot{\phi} = -\kappa(\mathbf{x},\mathbf{v})\mathbf{v}.\mathbf{v} \tag{5}$$

which is clearly negative definite for an appropriate form of potential. The function κ is defined to be positive definite and may be used to shape the rate of descent of the potential as a function of the vehicle position and/or velocity vectors. The system dynamics represented by Eq. (1b) may then be used with Eq. (4) to determine an appropriate choice of actuator inputs $\boldsymbol{\alpha}$.

Using this formulation it is seen that non-linear dynamical systems can be controlled using analytically derived functions. These control laws drive the system to the desired terminal state, which is evident from Eq. (5). Path constraints can be introduced by identifying such constrained regions with high potential. Therefore, since the rate of descent of the potential is guaranteed to be negative definite by the control laws, these undesired regions of the space are avoided. This property of the method will be used to enable active collision avoidance for a number of applications.

The convergence of the dynamical system to the desired state is shown schematically in fig. 1. In general the state space can be decomposed into a number of nested sets. Due to actuator saturation limits a convergence set can be defined within which all state space trajectories converge to the target

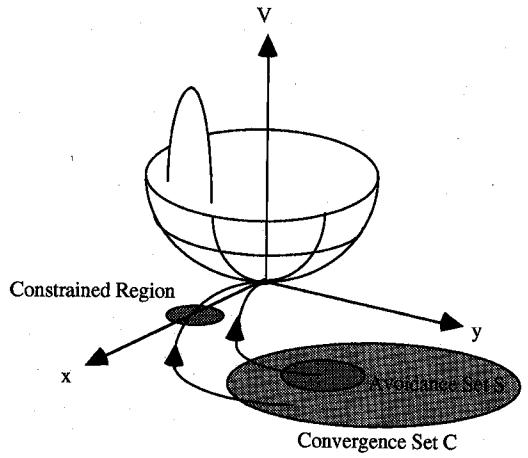

Fig. 1 Schematic potential field with convergence and avoidance sets.

state, defined as the global minimum of the potential field. Usually this global minimum corresponds to the vehicle being at rest at some desired generalised position vector. However, the terminal state may be a manifold representing a more complex final dynamical state. Within the convergence set there will exist an avoidance subset from which all state space trajectories not only converge to the desired terminal state, but do not intersect undesired regions of the state space. These may be physical obstructions, or may be more general undesired dynamical states. In principle, the potential function can be designed such that the convergence set and the avoidance set are equivalent.

Lastly, the regions of high potential can be considered to provide an imaginary 'repulsive force' acting to enforce the pre-defined path constraints. The magnitude of the potential field at the edge of the constrained region can be set equal to the potential at the initial vehicle state through the vector of parameters $\boldsymbol{\lambda}$. Therefore, since the rate of descent of the potential is negative definite, the vehicle cannot in principle enter the constrained region of the space. Although this appears to be a simple and attractive method, difficulties may arise for complex problems where local minima can arise in the potential field. While there are ad-hoc means of dealing with these difficulties a more elegant solution is the use of the Laplace equation to generate the potential field. In general, this requires the use of numerical methods with a grid solver to form the potential field. This extension of the method will be discussed later in section 2.4.

2.2 Discrete Control

For discrete control, such as impulsive thruster firings for translational control, a somewhat different implementation of the method is made. Again, a scalar potential field is defined, but it is now a function of the vehicle position vector only, viz.

$$\phi = \tfrac{1}{2}(\mathbf{x}-\tilde{\mathbf{x}})^{\mathrm{T}}\mathbf{M}(\mathbf{x}-\tilde{\mathbf{x}}) + V(\mathbf{x},\boldsymbol{\lambda}) \tag{6}$$

where the first term (which is in fact implicit in the continuous control formulation in the function V) ensures convergence to the desired goal location $\tilde{\mathbf{x}}$. The matrix of free parameters $\mathbf{M}$ may be used to shape the approach of the vehicle to the terminal state while the second term contains a representation of path constraints to be included in the control law. Again, the rate of descent of this function is given by

$$\dot{\phi} = \nabla\phi(\mathbf{x},\boldsymbol{\lambda}).\mathbf{v} \tag{7}$$

The vehicle dynamics are now freely propagated until the rate of descent of the potential vanishes. This condition then defines switching times for application of the discrete control, viz.

$$\dot{\phi} < 0 \quad \Rightarrow \quad s(t) = 0 \tag{8a}$$

$$\dot{\phi} \geq 0 \quad \Rightarrow \quad s(t) = 1 \tag{8b}$$

where the function $s(t)$ defines the control law switching times. When the controls are active, an impulsive change is made to the generalised velocity vector such that

$$\mathbf{v}^{-} + \Delta\mathbf{v} = -\kappa(\mathbf{x},\mathbf{v})\frac{\nabla\phi}{\|\nabla\phi\|} \quad \text{if} \quad s(t) = 1 \tag{9}$$

where $\mathbf{v}^{-}$ is the vehicle velocity vector immediately prior to the application of the impulse. Using the control defined by Eq. (9) the vehicle velocity vector is then directed down the potential gradient after application of the impulse. This ensures convergence to the goal since

$$\dot{\phi} = -\kappa(\mathbf{x},\mathbf{v})\|\nabla\phi\| \tag{10}$$

which, again, is negative definite for an appropriate form of potential field. Therefore, the vehicle converges to the desired terminal state with pre-defined path constraints enforced. Furthermore, the vehicle velocity magnitude can be shaped through the function κ to observe additional constraints. This is found to be most useful for docking and berthing problems where braking gates can be easily included along with path constraints.

2.3 Co-operative Control

The above analysis may be extended to problems with multiple spacecraft, for example co-operating free-flying spacecraft for inspection, active on-orbit servicing or on-orbit assembly. In this formulation the potential field is a function of the state of each of the N vehicles. In particular, the relative generalised position vector is used to ensure that the vehicles do not collide with each other during the co-operative manoeuvres. Analytic controls for the ith vehicle are now derived which are a function of the states of the other N-1 vehicles. This then leads to a naturally co-operative control method. The global potential field for a system of N spacecraft may be written as

$$\phi = \tfrac{1}{2}\sum_{i=1}^{N} \mathbf{v}_i.\mathbf{v}_i + \sum_{i=1}^{N}\sum_{j=1,j\neq i}^{N} V(\mathbf{x}_i - \mathbf{x}_j;\boldsymbol{\lambda}) \qquad (11)$$

Therefore, dropping the upper index on the summation, the rate of descent of the potential is found to be

$$\dot{\phi} = \sum_i \mathbf{v}_i.\dot{\mathbf{v}}_i + \sum_i \sum_j (\mathbf{v}_i - \mathbf{v}_j).\nabla V(\mathbf{x}_i - \mathbf{x}_j;\boldsymbol{\lambda}) \qquad (12)$$

However, it may be demonstrated that in the cases of interest the double summation may be re-written to allow Eq. (12) to be expressed as

$$\dot{\phi} = \sum_i \mathbf{v}_i.\dot{\mathbf{v}}_i + 2\sum_i \mathbf{v}_i.\sum_j \nabla V(\mathbf{x}_i - \mathbf{x}_j;\boldsymbol{\lambda}) \qquad (13)$$

Therefore, using the following control

$$\dot{\mathbf{v}}_i = -\kappa\mathbf{v}_i - 2\sum_j \nabla V(\mathbf{x}_i - \mathbf{x}_j;\boldsymbol{\lambda}) \qquad (14)$$

the rate of descent of the potential field is again rendered negative definite, viz.

$$\dot{\phi} = -\kappa\sum_i \mathbf{v}_i.\mathbf{v}_i \qquad (15)$$

Convergence of the group of spacecraft to some final desired configuration is then ensured for an appropriate form of potential. Furthermore, each vehicle reaches this state while observing the path constraints imposed by the other N-1 vehicles. Clearly this is of great importance for any co-operative group of free-flying inspection or servicing vehicles.

2.4 Local Minima Removal

A limitation of the potential field method is the appearance of local minima in the field for certain choices of parameter vector $\boldsymbol{\lambda}$. These local minima can lead to the vehicle being trapped in some state other than the desired terminal state. This problem can be alleviated by a number of ad-hoc means. For example, using the impulse control formulation the discrete nature of the control can lead to the vehicle being disturbed such that it escapes from any local minima. Alternatively, the potential can be constructed with a unique global minimum as a solution to Laplace's equation, viz.

$$\nabla^2\phi(\mathbf{x}) = 0 \qquad (16)$$

This equation has a family of solutions which will generate potential fields which are free of local minima [4]. However, for complex problems the Laplace equation must be solved using numerical methods. In particular the workspace must be modelled on a grid and a discrete version of the Laplace equation solved iteratively to form the potential field. This method of field generation will be discussed later in section 4.3.

3. ATV RENDEZVOUS AND DOCKING

3.1 The ATV Mission

A major application of the potential field method has been to studies of path constrained proximity manoeuvres, in particular for the ESA ATV spacecraft [6]. The ATV is an automated logistics supply vehicle for the ISS which will be launched by the Ariane-5E (E-Evolution) vehicle, beginning in 2003 (fig. 2). Its primary mission is to deliver a mix of cargo and propellant to the ISS, re-boost the ISS while docked and remove waste for destruction during re-entry. The ATV has a launch mass of up to 20 tons with a maximum cargo mass of 7.5 tons. The vehicle is injected into a 30 x 300 km orbit by Ariane-5E and then uses its primary propulsion system to rendezvous with the ISS after a number of phasing orbits. The final approach to the ISS, which initiates the proximity motion phase of the mission, begins at a waiting point some 2 km behind the station. The ATV then approaches the ISS through a series of way points using clusters of 220 N thrusters for attitude and translation control. Relative GPS navigation is used for the initial phase of the approach while laser sensors are used during the final approach within the V-bar (along the ISS orbit to

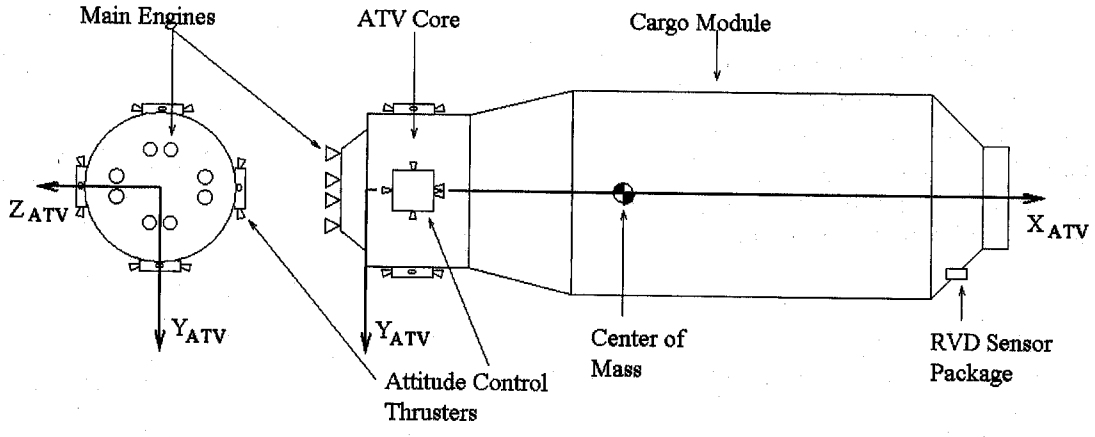

Fig. 2 ATV layout.

hard-dock at the Russian side of the station) and R-bar docking cones (along the radial direction from below the ISS to berth).

3.2 ATV Path Planning

As noted in section 3.1 the proximity phase of the ATV mission begins at a waiting point 2 km behind the ISS on the V-bar axis, as shown in fig. 3. This is the S_2 point which is used both as a hold point for system readiness checks before the final approach and to initiate the ATV Kalman filters used to provide relative GPS navigation. The S_2 point also defines the edge of the ISS approach ellipsoid. From S_2 the ATV manoeuvres to the W_1 waiting point 1 km behind the ISS on the V-bar axis. From here the ATV can manoeuvre along the V-bar axis to the W_2 point to perform a V-bar approach and hard-dock with the Russian side of the ISS at W_4, or the ATV can perform a fly-around to the W_3 point below the ISS to perform an R-bar approach to berth beneath the ISS at W_5. The trajectory segments T_i (i=1-9) represent various options for manoeuvring between the way points. While the ATV manoeuvres between way points it must stay outside a 200 m radius keep-out sphere centred on the ISS. The ATV may only enter the keep-out sphere through docking cones which penetrate the sphere along the V-bar and R-bar axes.

The ATV translational dynamics in proximity to the ISS can be represented by the Clohessey-Wiltshire equations [7]. Using a co-ordinate frame attached to the ISS, as shown in fig. 4, the linearised equations of motion of the ATV relative to the ISS may be written as

$$\ddot{x} + 2\omega\dot{y} = 0 \tag{17a}$$

$$\ddot{y} - 2\omega\dot{x} - 3\omega^2 y = 0 \tag{17b}$$

$$\ddot{z} + \omega^2 z = 0 \tag{17c}$$

where ω is the orbital angular velocity of the ISS. The discrete implementation of the potential field

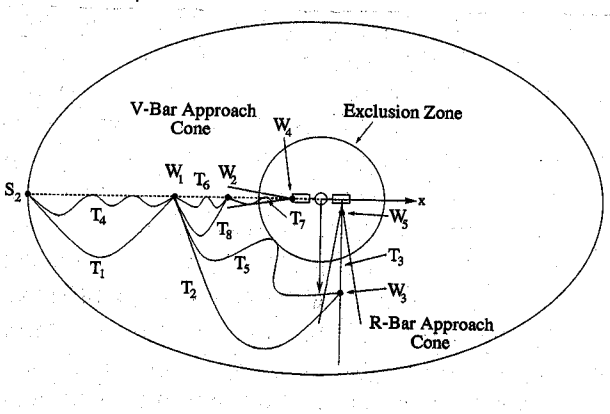

Fig. 3 ATV approach alternatives at the ISS.

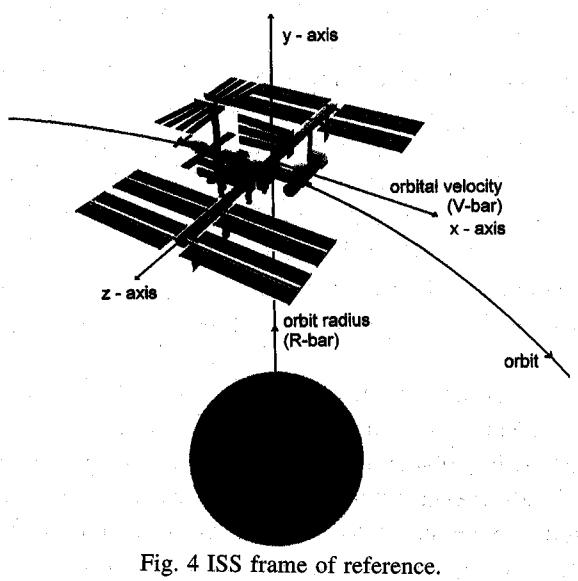

Fig. 4 ISS frame of reference.

method, discussed in section 2.2, will now be used as the basis of a control algorithm to manoeuvre the ATV to the ISS while enforcing path constraints [8]. In simulation additional effects are included in Eq. (17) to model the relative air drag of the ATV and ISS, the noise of the navigation system and thruster effects such as mis-alignment, minimum impulse bit and run-to-run variations [9,10].

In order to demonstrate the implementation of the method for proximity manoeuvring, a simple potential field of the form

$$\phi = \tfrac{1}{2}(\mathbf{x}-\tilde{\mathbf{x}})^{\mathrm{T}}\mathbf{M}(\mathbf{x}-\tilde{\mathbf{x}}),\ \mathbf{M} = \begin{bmatrix} m_1 & 0 & 0 \\ 0 & m_2 & 0 \\ 0 & 0 & m_3 \end{bmatrix} \qquad (18)$$

can be used to drive the ATV to some goal location $\tilde{\mathbf{x}}$. The matrix **M** is taken to be diagonal so that the potential is an ellipsoid with axes aligned with the co-ordinate frame attached to the ISS. The non-zero matrix elements may be used to shape the direction of the ATV approach to the goal point. Using the discrete implementation, the motion of the ATV is propagated using Eq. (17) until the rate of descent of the potential vanishes. Then, an impulse is applied which ensures that the motion of the ATV after the application of the impulse is down the local gradient of the potential field. The impulse $\Delta\mathbf{v}$ is applied such that

$$\mathbf{v}^{-} + \Delta\mathbf{v} = -\kappa(\mathbf{x},\mathbf{v})\frac{\nabla\phi}{\|\nabla\phi\|} \quad \text{if} \quad \dot{\phi} \geq 0 \qquad (19)$$

An unconstrained manoeuvre is shown in fig. 5 with the ATV starting from rest at the S_2 point and manoeuvring to the W_1 point with a spherical potential field using **M=I**, the identity matrix. By shaping the potential field using the matrix **M** to become ellipsoidal the trajectory segment can be shaped to force the ATV to manoeuvre closer to the V-bar axis. It can be seen from fig. 5. that the ATV is forced above the V-bar axis. This is contrary to conventional optimum two-impulse trajectories which use the natural relative motion provided by the orbital dynamics of the problem to effect the manoeuvre.

The same manoeuvre will now be considered again, but with path constraints. A single obstruction will be placed near the W_1 point representing an exclusion zone presented by a free-flying experiment platform, or some other transfer vehicle station-keeping near W_1. This constraint will be added

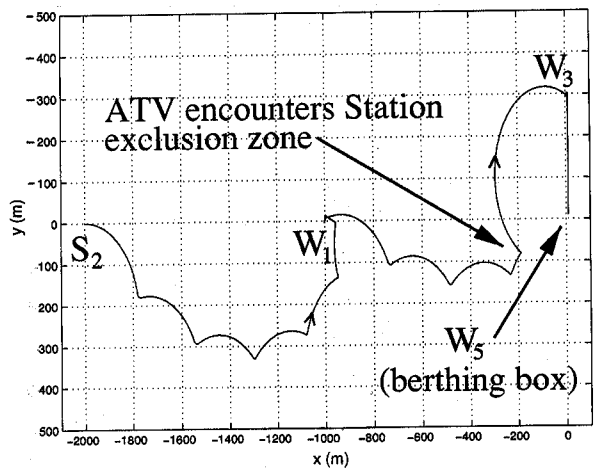

Fig. 5 ATV approach to the ISS from S_2 with an R-bar manoeuvre to berthing at W_5.

to Eq. (18) as a function of the form

$$\mathbf{V}(\mathbf{x},\tilde{\mathbf{x}};\lambda) = \lambda_1 \exp\{-\lambda_2(\mathbf{x}-\hat{\mathbf{x}})^{\mathrm{T}}\mathbf{N}(\mathbf{x}-\hat{\mathbf{x}})\} \qquad (20)$$

where $\hat{\mathbf{x}}$ is the location of the obstruction. Again the matrix **N** may be used to shape the potential field, with **N=I** representing a spherical exclusion zone. The potential field strength λ_1 and width λ_2 are used to ensure that the ATV cannot enter the excluded volume. This is achieved by choosing the potential at the edge of the excluded volume to be equal in magnitude to the ATV potential at the initial S_2 point. Therefore, since the control law ensures that the potential is continually decreasing, the ATV can never enter the excluded volume and so cannot collide with the obstruction, as shown in fig. 6. A similar collision avoidance manoeuvre is illustrated in fig. 5 which shows the ATV performing a manoeuvre to avoid the 200 m keep-out sphere centred on the ISS as it transfers from the W_1 waiting point to W_3 in preparation for an R-bar berthing below the station.

Along with path planning the potential field method can also be used to enforce braking gates during final approach to the ISS. The function $\kappa(\mathbf{x},\mathbf{v})$ in Eq. (19) can be defined as a set of analytic functions, or an interpolated look-up table used to control the approach speed of the ATV as a function of its location relative to the ISS. For example, the velocity profile for a series of braking steps is shown in fig. 7 for a V-bar approach where the x-coordinate is now measured locally from the docking port. During this phase the potential field must also keep the ATV positioned within a defined docking cone. Laser range, range-rate and attitude information is available during this terminal phase so that accurate

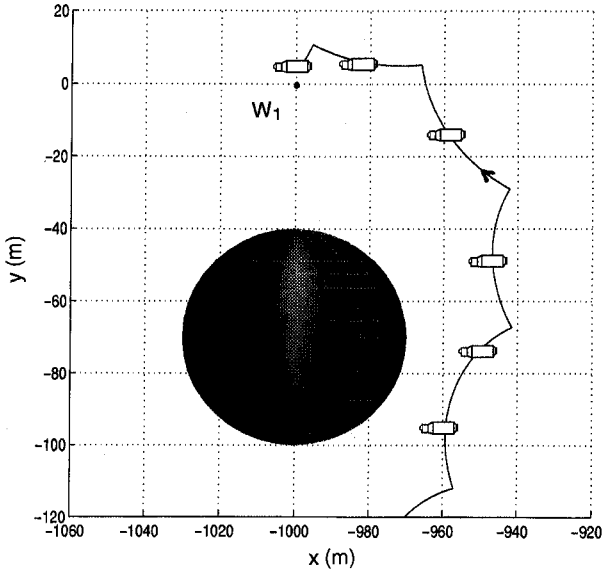

Fig. 6 Active collision avoidance at W_1.

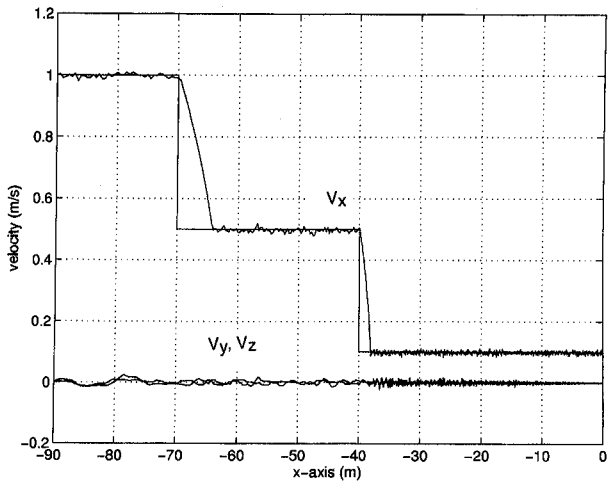

Fig. 7 Braking gates for a V-bar approach to hard-dock at W_4.

tracking of the braking steps is achieved. The final contact speed of 0.1 m s^{-1} is required to actuate the latches of the docking mechanism on the ATV and ISS. An alternative R-bar approach to the ATV berthing box is shown in fig. 5. Here approach speed constraints are again imposed along with a potential field to keep the ATV at the centre of the R-bar approach cone. For an R-bar approach the ATV is brought to rest in a berthing box and waits to be grappled by the station robot arm and attached to a berthing point below the ISS.

4. INSPECTOR MISSION PLANNING TOOLS

4.1 The Inspector Mission

The ISS Inspector is a free-flying camera being developed principally by Daimler-Chrysler Aerospace as an inspection tool for the ISS. The development programme is part of the NASA Pre-Planned Program Improvement (P^3I) for the station. The vehicle builds on the experience of the X-MIR Inspector mission of December 1997 which demonstrated video imaging of MIR from a free-flying camera [11]. The small 275 kg ISS Inspector will be delivered to the station by the space shuttle and attached to the ISS truss, possibly using an Express-type pallet as a customised docking port. The vehicle uses relative GPS and a laser ranger for navigation along with blocks of clod gas thrusters for attitude and translation control. The system functionality is completed by a Monitoring and Control Station (MCS) which is located in a standard equipment rack on-board the ISS. Future vehicles will include dextrous arms to allow for physical intervention during on-orbit servicing in addition to visual inspection.

The initial ISS Inspector vehicle will be used primarily for visual inspection of the station, as shown in fig. 8. Such remote inspection will allow full visual coverage of the exterior surfaces of the ISS to monitor the integrity of the structure, without the need for astronaut EVA. In addition to visual inspection, the vehicle can also accommodate a range of sensors to investigate the radiation and plasma environment in the vicinity of the ISS and to sense chemical leaks. The ISS Inspector can also perform these tasks for the space shuttle, when docked at the station.

The Inspector mission begins with a release and retreat from the docking port on the ISS, as shown in fig. 9. The vehicle is then transferred on to a passively safe fly-around ellipse at the S_2 way point (not the ATV way point notation). Passive safety is crucially important to ensure that the vehicle will drift away from the ISS in the event of communication loss or a failure of the propulsion system. The fly-around ellipse is configured such that the long term drift of the vehicle under the action of differential air

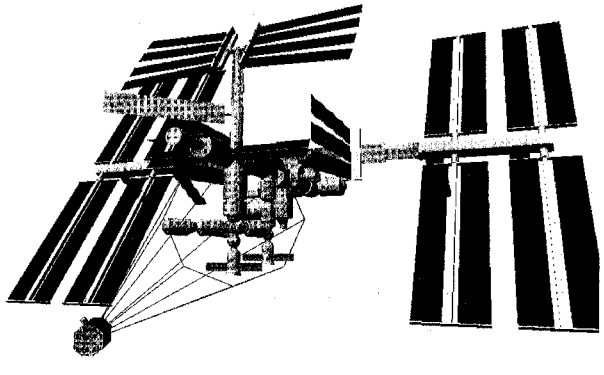

Fig. 8 Inspector observation of the ISS.

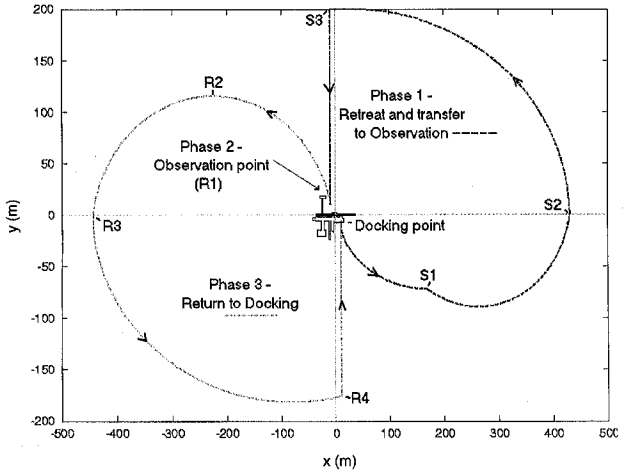

Fig. 9 Inspector mission phases.

drag does not induce a collision with the ISS, as shown in fig. 10. At an appropriate point on the fly-around ellipse the vehicle comes to rest, at way point S_3, and performs a passively safe R-bar approach to some desired observation point R_1. The vehicle then station-keeps at the observation point in order to make a visual inspection of the ISS before retreating through a series of way points and finally docking with the ISS using a second R-bar approach, again shown in fig. 9.

4.2 Mission Planning Tools

In order to select the mission observation point a number of operational constraints must be enforced. Firstly, the observation point must give a good view of the exterior region of the ISS which is of interest. In addition, the observation point at which the vehicle is station-keeping must be passively safe. In the event of a propulsion failure the resulting free-drift trajectory must not intersect the ISS. Similarly, the observation point must provide a clear line-of-sight for both UHF communications for command and higher frequency, high bandwidth communications for telemetering video. Since the radio frequency shadowing of the ISS structure is frequency dependent, the video link is more susceptible to fade than the command link. These constraints can be evaluated by the IMP (Inspector Mission Planner) software tool developed by the University of Glasgow. The software tool provides visualisation of the ISS as seen from the Inspector camera at varying focal lengths, as shown in fig. 11. The tool then uses the Clohessey-Wiltshire equations to propagate the free-drift motion of the Inspector and checks for collisions with the ISS structure. A screen icon indicates if the chosen observation point is indeed passively safe. Communications integrity is also checked by determining the line-of-sight from the Inspector to the command antenna fixed on the ISS. The link

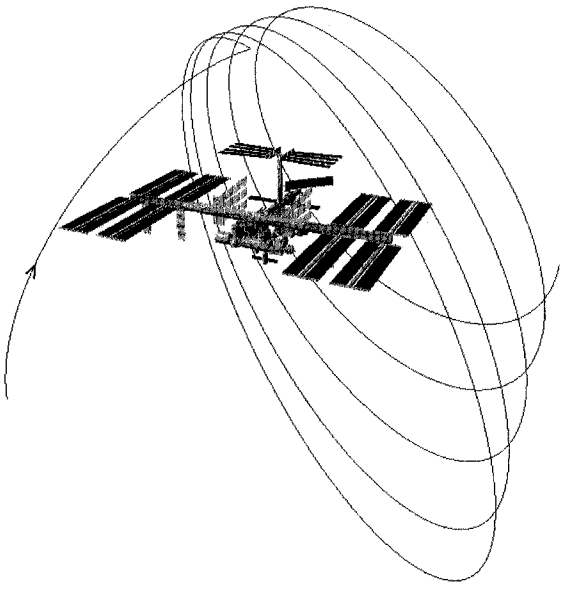

Fig. 10 Passively safe fly-around of the ISS.

integrity is checked for both command and video, again shown in fig. 11. Users of the IMP tool may be mission planners on the ground or astronauts on-board the ISS. By interfacing with the tool through mouse driven controls a suitable inspection point can be located which provides good viewing geometry along with a secure communications link and passive trajectory safety.

4.3 Path Planning Tools

While station-keeping at a fixed observation point is sufficient for some visual inspection tasks, the flex-

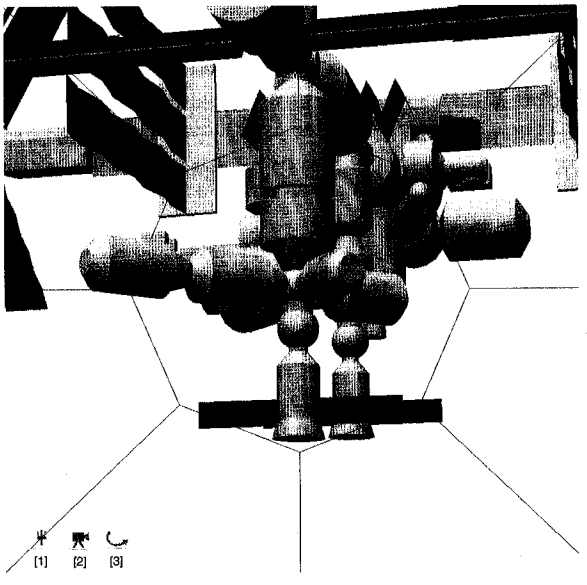

Fig. 11 ISS Inspector view: Icon [1] Command link integrity [2] Video link integrity [3] Passive safety confirmation.

ibility of the Inspector mission will be enhanced by active manoeuvring close to the ISS. Such capability will also be required for future Inspector vehicles which will be used for direct physical intervention using dextrous robot arms. However, active manoeuvring will inevitably require the use of trajectories, or trajectory segments, which are not passively safe. While this contravenes one of the major flight safety rules for the ISS, passive safety may be too strict a requirement in this instance. For example, the Inspector is of comparable mass to a fully suited astronaut on EVA with a large tool bag. Similarly, the maximum translational speed of the Inspector in the vicinity of the ISS is likely to be less than 0.1 m s^{-1}, which is also comparable to the speed of an astronaut on EVA moving along the ISS structure. Since the ISS structure, principally the module hulls, are designed to accommodate astronaut kick-loads during EVA, the kinetic energy imparted by a direct collision from Inspector is likely to be well within the expected loads during normal operation. Hence it may be possible to use a set of trajectory arcs which do not strictly satisfy the usual passive safety requirements.

In order to determine collision-free trajectories in close proximity to the ISS, a second mission planning tool has been developed. The FTP (Free-flyer Trajectory Planner) software tool uses a discretised form of the potential field method to generate collision-free trajectories between any two points in the vicinity of the ISS [12]. The method uses the Laplace equation to generate smooth potential fields which are free from local minima. For path planning in proximity to a complex structure such as the ISS, simple analytic potential fields cannot accurately capture the geometry of the workspace. The Laplace equation, discussed in section 2.4, must then be solved iteratively on a fine grid which accurately models the ISS structure. In discrete nodal form Eq. (16) may be written as

$$\phi_{i,j,k} = \tfrac{1}{6}[\phi_{i+1,j,k} + \phi_{i-1,j,k} + \phi_{i,j+1,k} + \phi_{i,j-1,k} + \phi_{i,j,k+1} + \phi_{i,j,k-1}] \qquad (21)$$

where $\phi_{i,j,k}$ is the potential at node (i,j,k) within the grid. In order to fully determine the potential field, the potential at the goal node is set to 0 while the potential at the nodes on the physical boundaries of the problem are set to 1. The potential at intermediate nodes is then obtained by propagating the Laplace equation through the grid using Eq. (21). Once the potential at each node is known, interpolation provides the entire potential field and its gradient. The switching algorithm defined by Eq. (9) is then used to force the free-flyer down the potential gradient to the goal point while enforcing active collision avoidance. Since the free-flyer is in close proximity to the ISS relative GPS information is unlikely to be available. It is assumed that a vision based navigation system is used whereby the free-flyer location is extracted by processing camera images.

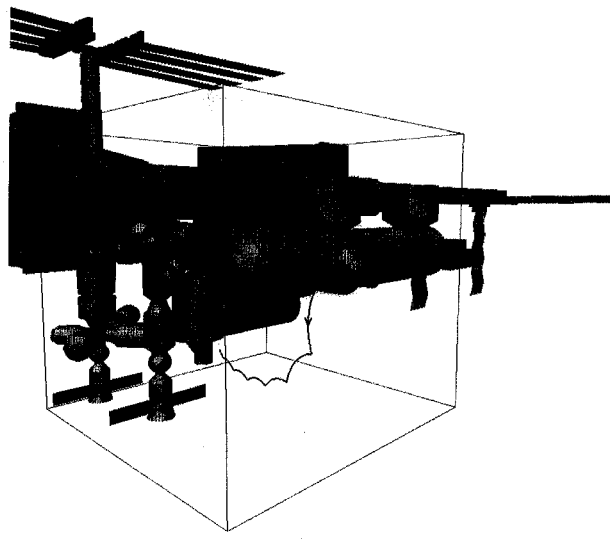

Fig. 12 ISS Inspector manoeuvre in close proximity to the ISS: beneath truss.

A typical manoeuvre is shown in fig. 12 where the ISS Inspector is initially station-keeping at an observation point close to the Columbus Orbital Facility (COF). Firstly, a control volume is established about the volume of space of interest. Then, a library with a geometric model of the ISS is called to generate the computational grid to be used to determine the potential field. The discretised form of the Laplace equation is then used to determine the potential field and the potential field gradient within the control volume. The interpolated field can then be used by the Inspector to safely manoeuvre from its initial observation point to some goal location, in this case beneath the station. A similar manoeuvre is shown in fig. 13 which shows the Inspector safely manoeuvring above the ISS to again reach some new observation point.

5. MICROCAMERAS FOR GEOSTATIONARY SATELLITES

The path planning tools discussed in section 4 are also relevant to the growing interest in the use of small free-flying micro-cameras for Geostationary satellite operations. This concept proposes the use of microspacecraft technology to develop 1 kg sized

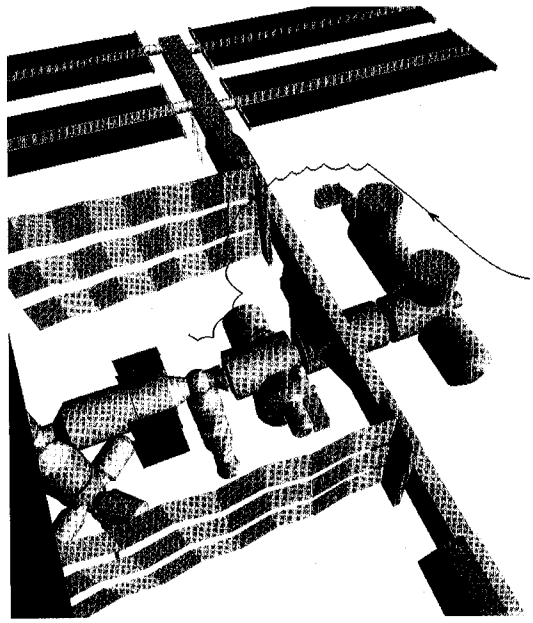

Fig. 13 ISS Inspector manoeuvre in close proximity to the ISS: above truss.

cameras to monitor the deployment of articulated components on large geostationary satellites, such as solar arrays and antennas [13]. The microcameras would be attached to the main satellite and deployed for visual inspection prior to and during mechanism deployment. At present the diagnostic information available during deployment failures is limited to data such as current-voltage telemetry from drive motors from which failure modes must be inferred. The availability of visual information may be of significant importance in recovering from deployment failures. Physical intervention may also be possible by using the free-flyer to gently collide with jammed mechanisms to aid deployment. A free-flyer trajectory in the vicinity of a large communication satellite is shown in fig. 14. Again, the mission planning and path planning tools developed for the ISS Inspector mission are suitable for this new application.

6. CO-OPERATIVE CONTROL OF MULTIPLE FREE-FLYERS

Along with single free-flying vehicles the potential field method may be used for the co-operative control of multiple free-flyers, as discussed in section 2.3. For example, on-orbit assembly of space structures has long been considered as a means of enabling the construction of large space platforms. Many scenarios envisage the use of free-flying robotic vehicles in the assembly process. It is found that the co-operative control method discussed in section 2.3 can enable the robotic assembly of regular geometric structures from a set of components using free-

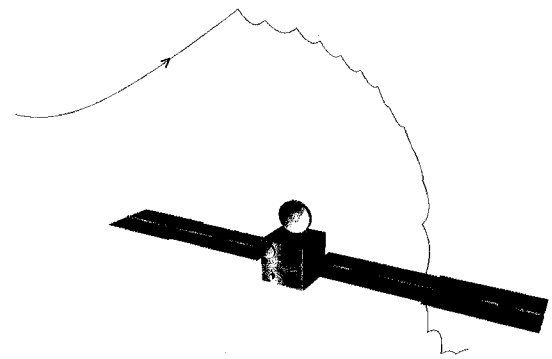

Fig. 14 Free-flyer trajectory in the vicinity of a large communication satellite.

flying dextrous robots [14,15]. By treating the ensemble of free-flying vehicles and components as a global system, a naturally co-operative control law is generated. The co-operative control law provides thruster switching times and impulse magnitudes for each free-flyer to ensure assembly of the components into some desired structure. The method enables complex assembly tasks to be achieved without recourse to artificial intelligence or rule-based schemes to drive the assembly process.

To extend the potential field method to enable the assembly of an arbitrary number of components requires the definition of a potential field encompassing all possible component connections within the structure. Therefore, an extended potential field termed the connection potential is now defined as

$$V_C = \tfrac{1}{2}\sum_{i=1}^{N}\sum_{j=1}^{N}\varepsilon_{ij}\left(\mathbf{r}_i - \tilde{\mathbf{r}}_j\right)\left(\mathbf{r}_i - \tilde{\mathbf{r}}_j\right) \qquad (22)$$

where the vector pair define the location of the ends of the ith component, as shown in fig. 15. The manner in which the individual components of the structure are connected is determined by the form of the connectivity matrix ε_{ij} which is constructed from the logic

$$\varepsilon_{ij} = \begin{cases} 1 & \text{Connection between } \mathbf{r}_i \text{ and } \tilde{\mathbf{r}}_j \\ 0 & \text{No connection between } \mathbf{r}_i \text{ and } \tilde{\mathbf{r}}_j \end{cases} \qquad (23)$$

where (i,j) corresponds to the element of column i and row j, read from the top left of the connectivity matrix. Therefore, a sparse matrix is obtained which consists solely of binary elements. For example, the connectivity matrix which corresponds to four linear beams connected in a square is given by

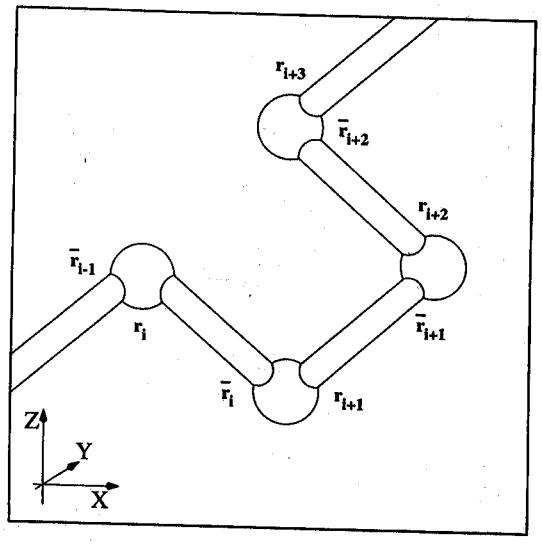

Fig. 15 Generic assembly of structural components.

$$\varepsilon_{ij} = \begin{Bmatrix} 0 & 1 & 0 & 0 \\ 0 & 0 & 1 & 0 \\ 0 & 0 & 0 & 1 \\ 1 & 0 & 0 & 0 \end{Bmatrix} \tag{24}$$

Reading from the top left, this particular matrix corresponds to beam 2 connecting to beam 1, beam 3 to beam 2, beam 4 to beam 3 and finally beam 1 to beam 4, closing the chain of the square. For a system consisting of many distinct components, a repulsive potential must be added to account for every possible combination of components resulting in a collision. Choosing a gaussian form, the global obstacle potential for collision avoidance is then defined as

$$V_0 = A \sum_{i=1}^{N} \sum_{j=1}^{N} \exp\left\{-B|\mathbf{r}_i^c - \mathbf{r}_j^c|\right\} \tag{25}$$

where $\mathbf{r}_i^c$ corresponds to the position of the geometric centre of the ith component of the structure. The potential field strength A is defined to be a function of the connection potential so that collision avoidance is gradually relaxed as the structure is assembled. This relaxation process is required to ensure that individual components of the structure can be connected.

As an example of the above formulation, the assembly of a cube will now be considered. The cube example demonstrates that the connectivity matrix formulation provides an elegant language for defining the assembly sequence for large structures. For example, the cube may be formed from the connectivity matrix for a square, defined by Eq. (24). The cube is simply two squares with a set of four parallel connectors. Therefore, the connectivity matrix for the square may be written as a large partitioned matrix, viz.

$$\varepsilon_{ij} = \begin{Bmatrix} \varepsilon_{ij}^{\,Square1} & \varepsilon_{ij}^{\,Connectors} & 0 \\ 0 & 0 & \varepsilon_{ij}^{\,Connectors} \\ 0 & 0 & \varepsilon_{ij}^{\,Square2} \end{Bmatrix} \tag{26}$$

This matrix formulation allows the generation of a library of basic structural forms which may then be appended by matrix manipulation. As the size of the connectivity matrix grows, it becomes impractical to connect every component in a single effort. Therefore a serial assembly sequence is required with a smaller number of free-flying robot assemblers than components. With a 12 x 12 connectivity matrix for the cube, the assembly must be staged. Dividing the connectivity matrix into three sections the full matrix defined by Eq. (26) becomes

$$\varepsilon_{ij} = \begin{array}{c} \begin{matrix} \quad I & & & & \quad II & & & & \quad III & & & \end{matrix} \\ \left\{\begin{array}{cccc|cccc|cccc} 0 & 1 & 0 & 0 & \mathbf{1} & 0 & 0 & 0 & 0 & 0 & 0 & 0 \\ 0 & 0 & 1 & 0 & 0 & \mathbf{1} & 0 & 0 & 0 & 0 & 0 & 0 \\ 0 & 0 & 0 & 1 & 0 & 0 & \mathbf{1} & 0 & 0 & 0 & 0 & 0 \\ 1 & 0 & 0 & 0 & 0 & 0 & 0 & \mathbf{1} & 0 & 0 & 0 & 0 \\ \hline 0 & 0 & 0 & 0 & 0 & 0 & 0 & 0 & \mathbf{1} & 0 & 0 & 0 \\ 0 & 0 & 0 & 0 & 0 & 0 & 0 & 0 & 0 & \mathbf{1} & 0 & 0 \\ 0 & 0 & 0 & 0 & 0 & 0 & 0 & 0 & 0 & 0 & \mathbf{1} & 0 \\ 0 & 0 & 0 & 0 & 0 & 0 & 0 & 0 & 0 & 0 & 0 & \mathbf{1} \\ \hline 0 & 0 & 0 & 0 & 0 & 0 & 0 & 0 & 0 & 1 & 0 & 0 \\ 0 & 0 & 0 & 0 & 0 & 0 & 0 & 0 & 0 & 0 & 1 & 0 \\ 0 & 0 & 0 & 0 & 0 & 0 & 0 & 0 & 0 & 0 & 0 & 1 \\ 0 & 0 & 0 & 0 & 0 & 0 & 0 & 0 & 1 & 0 & 0 & 0 \end{array}\right\} \end{array} \tag{27}$$

where section I represents to the assembly of a square base, section II represents the addition of the connecting beams (shown in bold) while section III corresponds to the final square structure required to complete the cube. The matrix is therefore read from the top left in four unit steps (corresponding to the assumed number of available free-flying assemblers) until the assembly sequence is complete at the bottom right. Implementing the potential in Eqs. (22), (25) with this matrix results in the assembly of the cube, as shown in fig. 16. As can be seen, the components are assembled into the desired cube structure in three distinct phases. From the basic cube more complex structural forms can also be

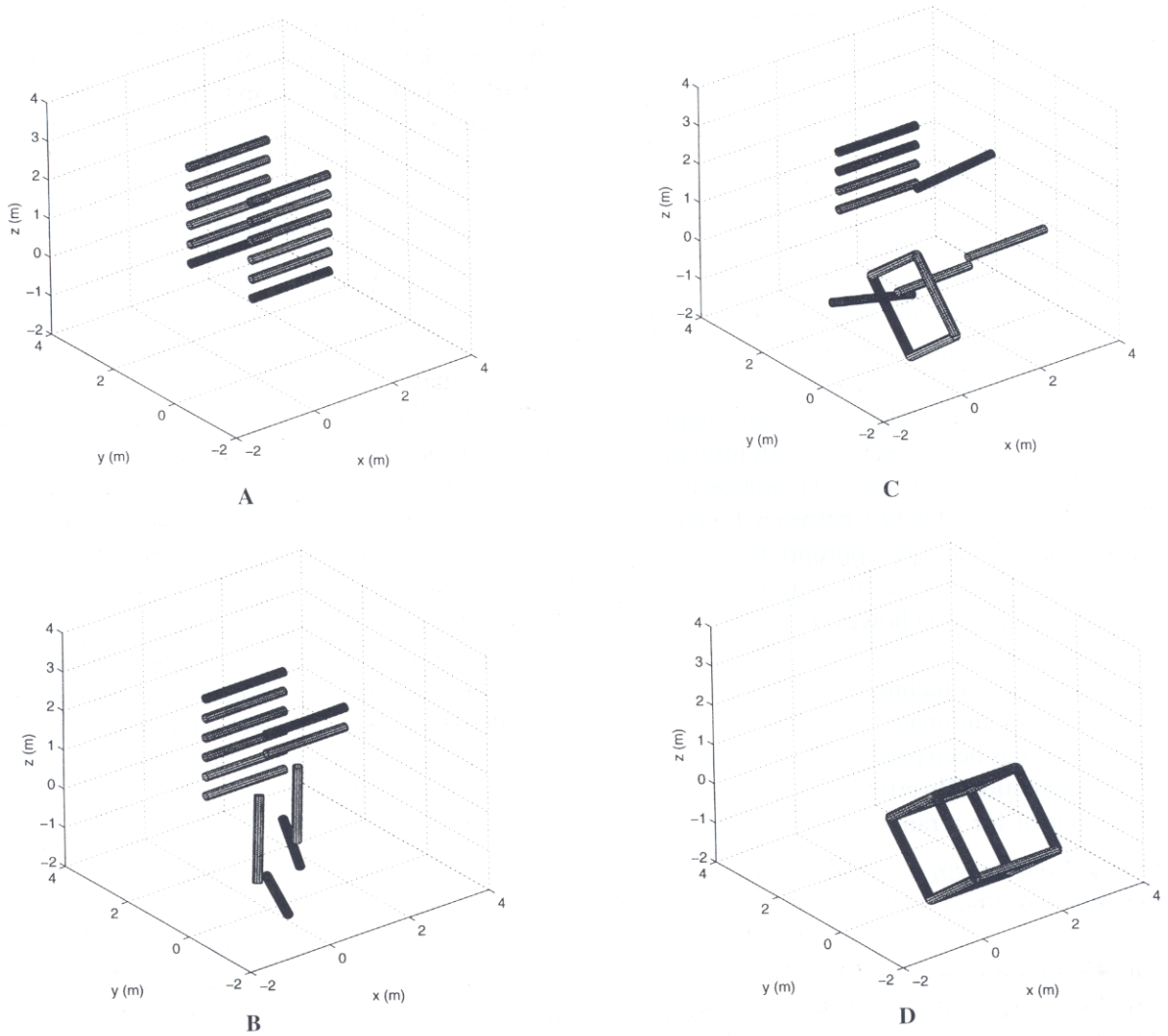

Fig. 16 Cube assembly **A.** t = 0 s **B.** t = 100 s **C.** t = 750 s **D.** t = 2900 s.

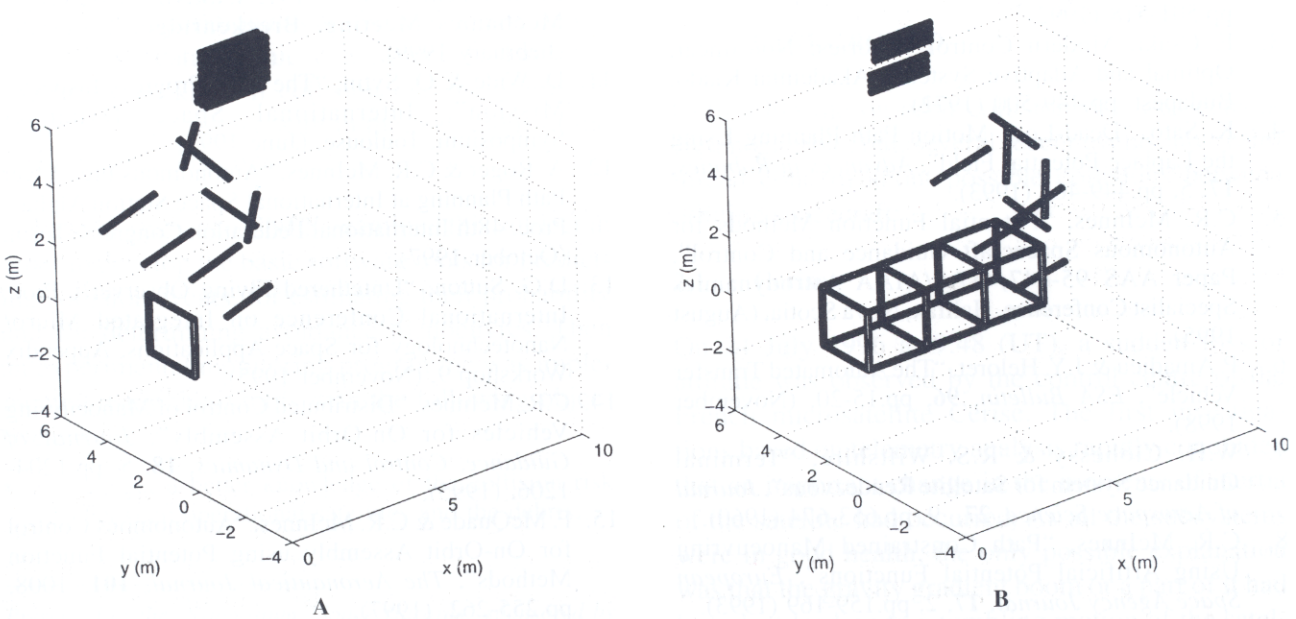

Fig.17 Truss assembly **A.** t = 1000 s **B.** t = 3750 s.

assembled. For example, the connectivity matrix for the cube can be appended to form a linear truss. The serial assembly of such a truss structure is shown in fig. 17.

7. CONCLUSIONS

While the debate concerning the relative merits of either human or robotic space exploration continues, it appears that the two are in fact complementary. Robotic free-flyers can perform many of the more mundane tasks currently requiring astronaut EVA. Similarly, future autonomous robots may enable on-orbit assembly of space structures with little human intervention. The future of space exploration is therefore likely to see a synergy between human and robot activities. What the appropriate balance is between these two activities to minimise cost still remains an open question however.

It is clear that a key technology for such activities is the provision of automated path planning tools. A generic method has been presented which provides a basis for computationally efficient autonomous guidance and control for a range of free-flying vehicle missions. Particular applications of the method to ATV rendezvous and docking at the ISS and path planning for the ISS Inspector have been discussed. In addition, an extension of the method has been considered for co-operative control of multiple free-flying robot assemblers. Future work will consider enhancements of the path planning tools to enable task planning and scheduling in addition to geometric trajectory planning. Such enhancements will be required to move towards fully autonomous free-flying robots for challenging future mission applications.

8. ACKNOWLEDGEMENTS

Part of the work contained within this paper was supported by funding from the European Space Research and Technology Centre Contract 11478/95/NL/JG(SC) supervised by Finn Ankersen and from Daimler-Chrysler Aerospace Space Infrastructure Division supervised by Detlef Wilde. The application development work was undertaken by Ender St-John Olcayto, Frank McQuade and Alexander Roger between 1995 and 1999.

REFERENCES

1. O.W. Olszewski, "Automated Terminal Guidance for a Shuttle Rendezvous to Space Station Freedom", Proc. AIAA Guidance, Navigation and Control Conference, AIAA, Washington DC, pp.337-387 (1990).
2. E. Rimon & D.E. Koditschek, "Exact Robot Navigation Using Artificial Potential Functions", *IEEE Trans. on Robotics and Automation*, **8**, 5, pp.501-518 (1992).
3. F. Csaki, Modern Control Theories: Non-linear, Optimal and Adaptive Systems, Akademiai Kiado, Budapest, pp.449-500 (1972).
4. K. Sato, "Dead-Lock Motion Path Planning Using the Laplace Potential Field", *Advances in Robotics*, **17**, 5, pp.449-461 (1993).
5. C.R. McInnes, "Potential Function Methods for Autonomous Spacecraft Guidance and Control", Paper AAS 95-447, AAS/AIAA Astrodynamics Specialist Conference, Halifax, Nova Scotia, (August 1995).
6. P. Amadieu & J.Y. Heloret, "The Automated Transfer Vehicle", *ESA Bulletin*, **96**, pp.15-20, (November 1998).
7. W.H. Clohessy & R.S. Wiltshire, "Terminal Guidance System for Satellite Rendezvous", *Journal of Aerospace Science*, **27**, 9, pp.653-674 (1960).
8. C.R. McInnes, "Path Constrained Manoeuvring Using Artificial Potential Functions", *European Space Agency Journal*, **17**, 2, pp.159-169 (1993).
9. E. Olcayto & C.R. McInnes, "Application of Potential Function Methods to Path Constrained Proximity Manoeuvring - Final Report", ESTEC 11478/95/NL/JQ/SC, (November 1997).
10. E. Olcayto, C.R. McInnes, F. Ankersen & J.Binder, "Control Design and Simulation of the Automated Transfer Vehicle within the MATLAB/Simulink Environment", AAS 99-141, AAS/AIAA Spaceflight Mechanics Meeting, Breckenridge, Colorado, (February 1999).
11. D. Wide & O. Sytin, "The MIR-Progress-Inspector Mission", International Space Dynamics Symposium, Toulouse, (June 1995).
12. A. Roger & C.R. McInnes, "Autonomous Free-Flyer Path Planning at International Space Station Alpha", Proc. 48th International Federation Congress, Turin, (October 1997).
13. D.G. Sutton, "Untethered Flying Observer", Proc. International Conference on Integrated Micro/Nanotechnology for Space Applications, Appendix Workshop 9, (November 1995).
14. C.R. McInnes, "Distributed Control of Manoeuvring Vehicles for On-Orbit Assembly", *Journal of Guidance, Control and Dynamics*, **18**, 5, pp.1204-1206, (1995).
15. F. McQuade & C.R. McInnes, "Autonomous Control for On-Orbit Assembly using Potential Function Methods", *The Aeronautical Journal*, **101**, 1008, pp.255-262, (1997).